

Labeling TiO₂ Nanoparticles with Dyes for Optical Fluorescence Microscopy and Determination of TiO₂-DNA Nanoconjugate Stability

Kenneth T. Thurn, Tatjana Paunesku, Aiguo Wu, Eric M. B. Brown, Barry Lai, Stefan Vogt, Jörg Maser, Mohammed Aslam, Vinayak Dravid, Raymond Bergan, and Gayle E. Woloschak*

Visualization of nanoparticles without intrinsic optical fluorescence properties is a significant problem when performing intracellular studies. Such is the case with titanium dioxide (TiO₂) nanoparticles. These nanoparticles, when electronically linked to single-stranded DNA oligonucleotides, have been proposed to be used both as gene knockout devices and as possible tumor imaging agents. By interacting with complementary target sequences in living cells, these photoinducible TiO₂-DNA nanoconjugates have the potential to cleave intracellular genomic DNA in a sequence specific and inducible manner. The nanoconjugates also become detectable by magnetic resonance imaging with the addition of gadolinium Gd(III) contrast agents. Herein two approaches for labeling TiO₂ nanoparticles and TiO₂-DNA nanoconjugates with optically fluorescent agents are described. This permits direct quantification of fluorescently labeled TiO₂ nanoparticle uptake in a large population of living cells (>10⁴ cells). X-ray fluorescence microscopy (XFM) is combined with fluorescent microscopy to determine the relative intracellular stability of the nanoconjugates and used to quantify intracellular nanoparticles. Imaging the DNA component of the TiO₂-DNA nanoconjugate by fluorescent confocal microscopy within the same cell shows an overlap with the titanium signal as mapped by XFM. This strongly implies the intracellular integrity of the TiO₂-DNA nanoconjugates in malignant cells.

Keywords:

- DNA
- X-ray fluorescence microscopy
- nanoconjugates
- nanoparticles
- TiO₂

[*] Prof. G. E. Woloschak
Departments of Radiation Oncology, Radiology, and Cell and
Molecular Biology
Northwestern University Feinberg School of Medicine
Chicago, IL 60611 (USA)
E-mail: g-woloschak@northwestern.edu

K. T. Thurn, Prof. T. Paunesku, Dr. A. Wu, E. M. B. Brown
Department of Radiation Oncology
Northwestern University Feinberg School of Medicine
Chicago, IL 60611 (USA)

Dr. B. Lai, Dr. S. Vogt
X-Ray Science Division, Advanced Photon Source
Argonne National Laboratory
Argonne, IL 60439 (USA)

Dr. J. Maser
Center for Nanoscale Materials, Advanced Photon Source
Argonne National Laboratory
Argonne, IL 60439 (USA)

Dr. M. Aslam
Department of Physics
Indian Institute of Technology Bombay Powai
Mumbai 400076 (India)
Prof. V. Dravid
Department of Material Science and Engineering and
NUANCE Center
Northwestern University
Evanston, IL 60208 (USA)

Prof. R. Bergan
Department of Medicine
Robert H. Lurie Cancer Center
Northwestern University Feinberg School of Medicine
Chicago, IL 60611 (USA)

DOI: 10.1002/sml.200801458

1. Introduction

Some of the most examined nanoparticles to date are those composed of titanium dioxide due to their unique photocatalytic and structural properties. TiO₂ nanoparticles have been investigated for potential uses as disinfectants,^[1–3] diagnostic assays,^[4] biological probes,^[5] tumor cell killing agents,^[6–8] and even for gene targeting.^[9–11] These nanoparticles make an attractive mechanism to target cancer cells since photoactivation of TiO₂ (1000 μg mL⁻¹) with energies of 3.2 eV causes a release of reactive oxygen species (ROS).^[12] Photoexcited TiO₂ nanoparticles were shown to cause significant cell death in various cancer cell lines.^[6–8] While the bulk form of TiO₂ is considered generally biologically inert,^[1] there is some controversy as to the extent of TiO₂ nanoparticle cytotoxicity.^[8,13–16] Recently, however, intravenous tail-vein injection of 5 mg kg⁻¹ of TiO₂ nanoparticles (<100 nm) into male Wistar rats showed no deleterious effects on organ function and caused no detectable inflammatory response *in vivo*.^[17]

Our laboratory is investigating the use of TiO₂ nanoparticles bound to single-stranded DNA oligonucleotides creating TiO₂–DNA nanoconjugates. Reduction of particle size below 20 nm results in TiO₂ surface corner defects that can be repaired through covalent bonds with ortho-substituted enediol ligands (e.g., dopamine, alizarin) forming stable charge transfer complexes.^[18–20] The TiO₂–DNA nanoconjugates are being examined as potential gene targeting devices, and imaging agents for the detection of tumors. The nanoconjugate consists of a TiO₂ nanoparticle covalently bound to dopamine, which is itself bound to a single-stranded DNA oligonucleotide (Figure 1).^[9] The DNA maintains its sequence-specific hybridization, while the nanoparticle component maintains its photocatalytic properties.^[9,20] When photoactivated, a charge separation occurs within the nanoparticle, resulting in the migration of an electropositive hole (h⁺) from the nanoparticle, through the dopamine, and onto the DNA^[20,21] finally resulting in its scission.^[9] Therefore, TiO₂–DNA nanoconjugates should be able to specifically cleave mutated genomic DNA in a sequence-specific and inducible manner. In this way, they have the potential to specifically and effectively target oncogenes that represent desirable therapeutic targets (e.g., ras, myc).^[22–25] By conjugating dopamine modified gadolinium Gd(III) contrast agents directly to the surface of the TiO₂ nanoparticle, the nanoconjugates become detectable by T₁-weighted magnetic resonance imaging (MRI),^[26,27] therefore possibly allowing *in vivo* detection of tumors.

Despite extensive research into the interaction between cells and TiO₂ nanoparticles, the lack of variety in techniques to allow *in vitro* and *in vivo* TiO₂ detection has hindered statistical analysis of large-scale cell–TiO₂ nanoparticle interaction studies. Most studies to date rely primarily on transmission electron microscopy (TEM) to determine nanoparticle internalization, and some verify this with energy-filtering TEM (EFTEM).^[13,14,28,29] Despite the high spatial resolution of these techniques they only permit analysis of relatively small cell numbers, and require sectioning of the biological samples. TiO₂ nanoparticles have recently been

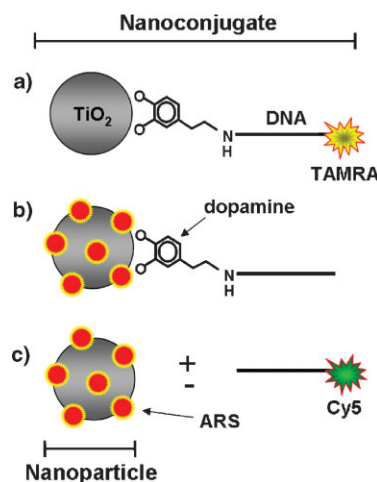


Figure 1. Schematic representation of fluorescent labeling of TiO₂–DNA nanoconjugates. a) DNA oligonucleotides are 3' labeled with tetramethylrhodamine (TAMRA), while the 5' carboxyl dT terminal end is modified with dopamine which subsequently binds the surface defects of TiO₂ nanoparticles (<20 nm). b) Direct covalent conjugation of Alizarin Red 5 (ARS) to the undercoordinated surface defects of TiO₂ nanoparticles creating an ARS-labeled TiO₂–DNA nanoconjugates. c) Direct ARS labeling of nanoparticle with the addition of free, unbound Cy5-labeled DNA oligonucleotides.

conjugated to 5-maleimide fluorescein dyes,^[8] but fluorescein can be quenched upon binding of the TiO₂ nanoparticle with enediol ligands (e.g., dopamine).^[4] It is also possible to detect a change in side-scatter characteristics of cell populations using flow cytometry as a function of TiO₂ nanoparticle uptake.^[30] Since, however, side scatter is only an indicator of cell granularity^[31] it cannot directly detect the nanoparticles themselves, and thus requires treatment with relatively high numbers of nanoparticles. Therefore additional methods for detecting intracellular TiO₂ are greatly needed.

Recently, our group has used X-ray fluorescence microscopy (XFM) to detect and map nanoparticles directly in whole cells based on their titanium content.^[9,10] XFM is a powerful and sensitive technique (which detects as few as several thousand atoms^[32]) using bright X-rays to excite element specific K α X-ray fluorescence and create a quantitative and qualitative elemental map of biological samples at submicron resolutions.^[32–35]

Using XFM and TEM, our group has shown that the TiO₂–DNA nanoconjugates can be specifically retained in subcellular compartments where complementary nuclear or mitochondrial DNA is present.^[9,10] It is crucial for further investigations of TiO₂ that large populations of cells be examined rapidly and consistently. In order to achieve this goal we devised methods to modify the TiO₂ nanoparticle with optical fluorescent dyes which are normally invisible by optical microscopy except at very high quantities. We have accomplished this by using fluorescently labeled DNA oligonucleotides, and by labeling the nanoparticles directly with Alizarin Red S (ARS). The ARS surface modification can be performed either before or after nanoparticles have been taken up by cells. Subsequently, this permitted the use of high throughput techniques such as flow cytometry to quantify

cellular uptake of nanoparticles. It also allowed direct investigation into the cytotoxicity of nanoparticles in conjunction with nanoparticle uptake. Fluorescent modification of nanoparticles combined with XFM allowed determination of the relative intracellular TiO_2 -DNA nanoconjugate stability.

2. Results and Discussion

One of the limiting factors in TiO_2 nanoparticle studies is the lack of diversity in available intracellular detection techniques. Taking advantage of the surface chemistry of TiO_2 nanoparticles, the nanoparticle/nanoconjugates were fluorescently labeled by two separate approaches. At 20 nm or below, the metal oxide nanoparticles' surface geometry changes from a pentacoordinated to a hexacoordinated position.^[19] These undercoordinated "surface defects" have a high affinity for ortho-substituted enediol ligands (e.g., dopamine, alizarin, ascorbic acid) that restore the surface titanium atom's coordination back to its relaxed, octahedral form upon binding.^[19,36] DNA oligonucleotides that had their 5' dT terminal ends carboxyl modified, were bound to dopamine as described earlier.^[9,10,20] Their 3' terminal ends were labeled with either fluorescent tetramethylrhodamine (TAMRA) or Cy5. The 5' dopamine modified end was then used to covalently link the DNA oligonucleotide directly to the surface of the nanoparticle creating a stable TiO_2 -dopamine-DNA nanoconjugate with a fluorescently labeled nucleic acid component (Figure 1).

In an attempt to establish a simple, inexpensive, and covalent process to fluorescently label the nanoparticle directly for intracellular detection, we modified the surface of the metal-oxide nanoparticles with Alizarin Red S (ARS). We suspected that binding of ARS to nanoparticles would render them highly fluorescent since locally high concentrations of ARS molecules increase their local concentration and light absorbance. ARS (a derivative of alizarin) is an ortho-substituted enediol ligand that has never been previously reported to be used as an intracellular label for TiO_2 nanoparticles. ARS has been used in optical microscopy for fluorescent labeling of calcium deposits.^[37,38] Since the same hydroxyl groups of ARS are significant in the binding to both calcium and TiO_2 ,^[38] the nanoparticle bound ARS should be precluded from binding calcium. It has been reported that ARS is able to form complexes with proteins at low pH (3.6), although this was almost completely inhibited as pH values approached physiological conditions.^[39] For direct surface binding to the nanoparticle, ARS was added to 5 nm TiO_2 nanoparticles. The nanoparticles' UV/vis absorbance spectra were analyzed since surface modification of the nanoparticle will cause a change in absorbance. Results from Figure 2 show that TiO_2 nanoparticles show absorption wavelengths smaller than 350 nm. Conjugation of 44% of the total surface titanium atoms with ARS (TiO_2 -ARS) caused a red shift and creation of a unique absorption maximum at 510 nm. This fluorescence could be excited at relatively long wavelengths (absorption peak at 510 nm is very broad), which have higher tissue/cell penetrance than the UV wavelengths. The UV/vis absorbance spectra of the TiO_2 -ARS complex were very similar to those published of TiO_2 -Alizarin.^[18,40] This is not

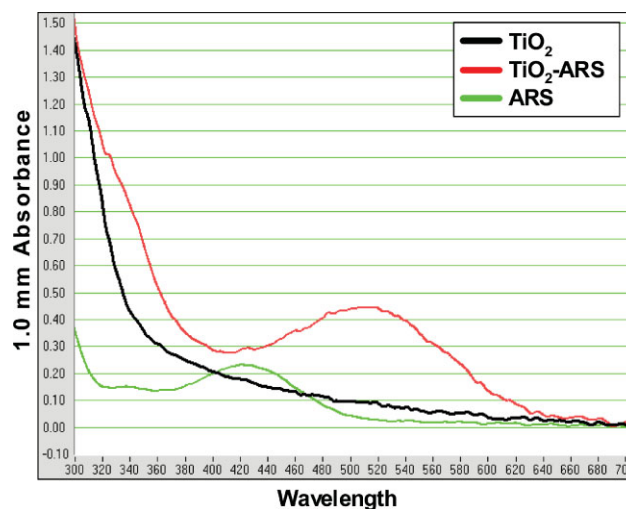


Figure 2. UV/vis absorbance spectrum of TiO_2 -, ARS-, and ARS-coated TiO_2 nanoparticles. TiO_2 nanoparticles (5 μM) showed an onset of absorption near 350 nm. The addition of ARS (0.9 mM) to nanoparticles (TiO_2 -ARS), coating approximately 44% of the surface titanium atoms, resulted in a distinct absorbance maximum at approximately 510 nm. ARS alone also at 0.9 mM had an absorbance peak at 420 nm.

surprising since the two polycyclic aromatic molecules differ only in the addition of a sulfonate group on ARS (1,2-dihydroxyanthraquinone vs. 1,2-dihydroxyanthraquinone-3-sulfonate). ARS alone at the same concentration had an absorbance peak at 420 nm. To determine if the ARS modified nanoparticles in cells are detectable by fluorescent confocal microscopy, prostate cancer PC-3M and breast cancer MCF-7 cells were serum-starved and treated with ARS coated TiO_2 nanoparticles (TiO_2 -ARS). As controls, cells were left untreated, treated with ARS alone, or treated with uncoated TiO_2 . Absolute ARS and nanoparticle concentrations were the same in each case. The treated cells were then imaged using two separate excitation lasers: 488 nm and 543 nm. A previous study claimed to have detected TiO_2 nanoparticles directly using an excitation laser of 488 nm with emission filters between 505–550 nm.^[30] Figure 3A, third row, shows the results when similar experimental and microscopy parameters were used. Cells were treated with the nanoparticles, which lead to a significant accumulation of nanoparticles on the cell surface as well as internalized nanoparticles. It is noteworthy that in all further experiments we used an acidic glycine wash (200 mM, pH 4.0) in order to decrease surface bound nanoparticles. Extensive washing in low-pH glycine was demonstrated to reduce oligonucleotide binding to the cell surface.^[41] We found that it also significantly reduced the extent of nanoparticle binding to the cell membrane (data not shown). Unlabeled TiO_2 nanoparticles did not exhibit a detectable fluorescent signal using a 488 nm excitation laser and a 505–530 nm bandpass filter for signal detection. The difference compared to the previous study^[30] may perhaps be caused by different properties/sizes of nanoparticles (23 nm versus 5 nm), different degrees of nanoparticle accumulation within cells, or different degrees of background fluorescence. Treatment of cells with TiO_2 -ARS (fourth row) did, however, result in a strong fluorescent signal in the range of 560–615 nm when excited with a 543-nm laser. Thus ARS modified nanoparticles are fluorescent emitting at

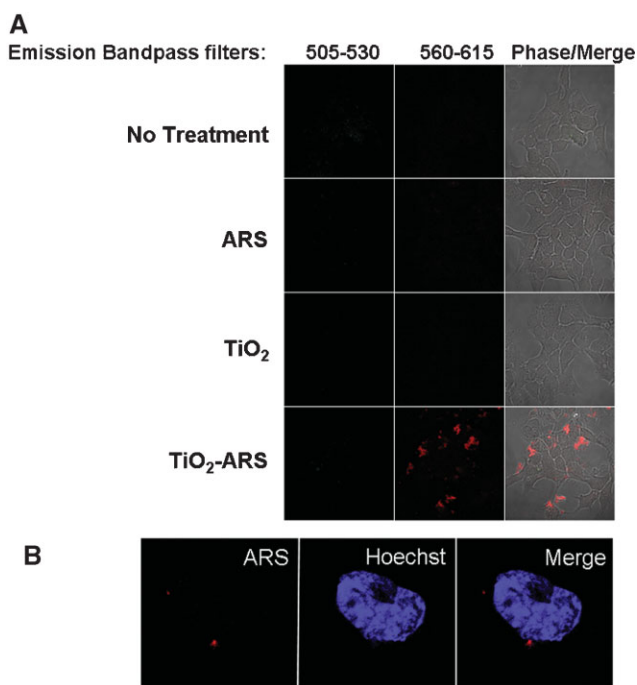


Figure 3. Intracellular detection of ARS modified TiO₂ nanoparticles. A) PC-3M cells were either untreated, treated with 60 μM ARS, or treated with 333 nm of TiO₂ nanoparticles that were either unmodified (TiO₂) or ARS-coated (TiO₂-ARS). A strong fluorescent signal was only detected in cells treated with nanoparticles modified with ARS, using a 560–615-nm band-pass filter (excitation = 543 nm). B) Labeling intracellular TiO₂ nanoparticles in fixed cells. Cells were treated with unlabeled TiO₂ nanoparticles, washed, fixed, and stained with Hoechst 33342 to label the nucleus (blue). Then cells were treated with 0.9 mM ARS (red) in PBS to label the already internalized nanoparticles.

560–615-nm wavelengths where little background fluorescence can be expected. Importantly, cells treated with ARS alone did not produce a detectable fluorescent signal with either excitation laser. Non-specific retention of ARS did not occur within the cells under the conditions tested, and ARS was not able to form significant fluorescent intracellular complexes without conjugation to the TiO₂ nanoparticle.

In order to determine if post-treatment fluorescent labeling of nanoparticles already internalized into cells with ARS was possible, PC-3M cells were treated with unlabeled nanoparticles, fixed, and subsequently stained with an ARS solution in phosphate buffered saline solution (PBS). Results in Figure 3B show a detectable intracellular ARS fluorescence within the cytoplasm. Fixed cells that were not previously treated with TiO₂ did not exhibit a detectable fluorescent signal upon treatment with the ARS solution (Figure 3A). This suggests that internalization of nanoparticles was not due to ARS coating, and that ARS was able to bind intracellular TiO₂ particles in fixed cells.

Our group has previously conjugated glycidyl isopropyl ether (GIE) to the surface of TiO₂ nanoparticles (TiO₂-GIE) in order to reduce bioreactivity of the nanoparticle within cells.^[9,10] The use of uncoated TiO₂ nanoparticles is also of significance since their excitation produces an abundance of reactive oxygen species which can be used for cell killing without gene specific targeting.^[6,8] Therefore, we determined

the viability of cells that have taken up GIE coated or uncoated TiO₂ nanoparticles. Viability assays require investigation of thousands of cells and could never be done in conjunction with TEM or XFM. Labeling the nanoparticles, however, allowed us to screen the treated cells simultaneously for nanoparticle uptake (by ARS fluorescence) and for viability (by use of fluorescent live-cell-impermeable dye). PC-3M cells were treated with GIE coated and uncoated TiO₂ nanoparticles labeled with ARS. As a control, 20 mM hydrogen peroxide (H₂O₂) was used as an inducer of cell death.^[42] Flow cytometry was then used to quantify both the extent of nanoparticle uptake within the cell population, and the cells' ability to exclude cell-impermeable DAPI as an indicator of cell viability. Results show that when treated with ARS alone, virtually the entire population of cells was viable and capable of dye exclusion (Figure 4A). Both of the TiO₂ nanoparticle-treated cell populations (TiO₂-GIE-ARS and TiO₂-ARS) showed no significant decrease in viability, with the number of dead cells averaging 5% and 2%, respectively (*n* = 3). H₂O₂ treated cells, on the other hand, showed an approximately 54% reduction in viability. This suggested that neither TiO₂-ARS nor TiO₂-GIE-ARS nanoparticles had a significant effect on cell viability at the concentration used in the experiments described herein. These results were confirmed in MCF-7 cells (data not shown).

While simultaneously detecting cell viability, samples were also analyzed for ARS fluorescence as an indicator of nanoparticle uptake. Internalization of nanoparticles was shown by the number of cells excited to fluoresce using similar parameters to those performed during microscopy. Figure 4B is a representative plot of several experiments performed (*n* = 3), showing that cells treated with ARS alone exhibited very low autofluorescence (excitation with 543-nm laser, emission in 560–615-nm range). Cells treated with TiO₂-GIE-ARS showed an average nanoparticle uptake of 36% within the cell population, while TiO₂-ARS nanoparticles lacking GIE had a similar nanoparticle internalization of 32%. This suggested that GIE did not significantly aid in the internalization of the nanoparticle, nor did it affect viability of cells. Importantly, ARS could be used by both confocal microscopy and flow cytometry to detect intracellular TiO₂-ARS nanoparticles.

To determine the subcellular localization of the separate components of the TiO₂-DNA nanoconjugates, cells were treated simultaneously with both TiO₂-ARS nanoparticles and free Cy5-labeled unbound DNA oligonucleotides. After treatment and washes, the cells were imaged by confocal microscopy. Results in Figure 5 show that there was a strong accumulation of the ARS labeled nanoparticles in endosomal vesicles within the cytoplasm. Although it is possible that the endocytic mechanisms of TiO₂ nanoparticles change due to ARS labeling, the subcellular distribution was similar to that seen when the Alizarin Red S was used for post-treatment staining (Figure 3B); in addition, work by others with unlabeled nanoparticles using TEM showed similar nanoparticle distribution.^[14] This would suggest that the uptake mechanism was not altered due to Alizarin Red S surface labeling. The free oligonucleotides, on the other hand, showed a strong localization within the nuclei, and more strikingly

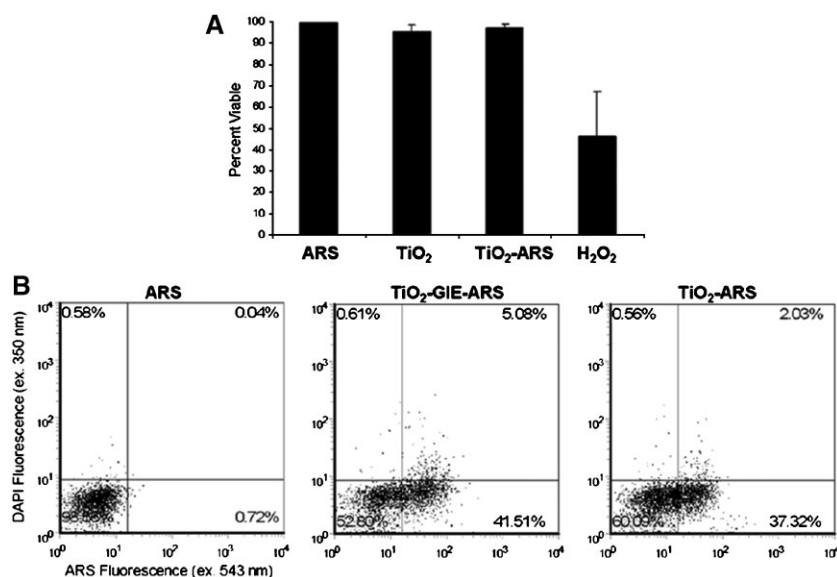


Figure 4. TiO₂ nanoparticles uptake and effect on cell viability. A) PC-3M cells were treated with 60 μM ARS, 333 nm ARS-labeled GIE-coated nanoparticles (TiO₂-GIE), ARS-labeled uncoated TiO₂ nanoparticles (TiO₂-ARS), or 20 mM hydrogen peroxide (H₂O₂) for 24 h. Cell samples were analyzed for their ability to exclude DAPI as a function of cell viability. B) A representative plot obtained from one of three independent experiments. Uptake of ARS labeled TiO₂ nanoparticles was analyzed in the same cells from (A). ARS fluorescence (em. 560–615 nm, ex. 543 nm) was used as an indicator of nanoparticle uptake and plotted against DAPI as an indicator of cell death.

within the nucleoli. This was similar to the results previously obtained with free oligonucleotides^[43–45] and by our group with complete nanoconjugates.^[9,10] These results demonstrated that the separate components of the nanoconjugates (the nanoparticle and DNA oligonucleotide) accumulated in separate subcellular organelles and did not co-localize within the same cell if not covalently bound together. This suggests that the separate components enter the cell via unique

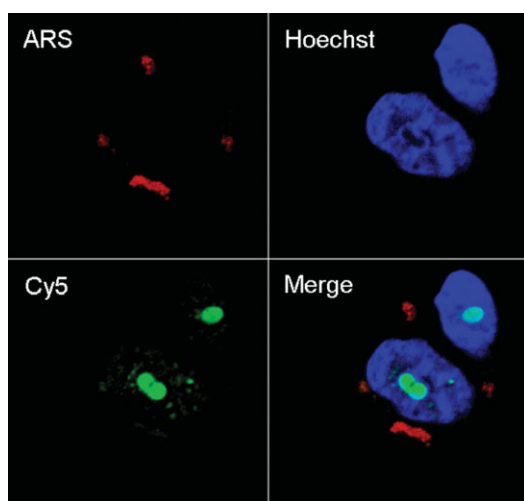


Figure 5. Localization of TiO₂ nanoparticle uptake versus free unbound DNA oligonucleotides. Serum starved cells were treated for 1 h with 333 nm of ARS-coated TiO₂ nanoparticles and 160 μM of free unbound Cy5 labeled oligonucleotides to determine the subcellular localization of each component separately.

internalization mechanisms, or are distinctly trafficked within the cell. Although these mechanisms have been extensively studied for oligonucleotides in various cell lines,^[46–49] this is not the case for TiO₂ nanoparticles. Further experiments aimed at determining these mechanisms are vitally needed since the modes of trafficking and internalization have a direct impact on subcellular localization and potential cytotoxicity. Since the functionality and targeting of the nanoconjugates are greatly dependent on their integrity, we combined confocal microscopy with XFM to track both components independently within the same cell. Confocal microscopy was used to detect the DNA oligonucleotide component, while XFM was used to directly detect titanium (and thereby the nanoparticles). XFM was performed at the 2-ID-D beamline at the Advanced Photon Source at Argonne National Laboratories. XFM mapped the location and concentration of elements ranging from phosphorus to zinc on the periodic table (including titanium) using raster scanning with step sizes of 0.3 μm.

Figure 6A shows the results from confocal microscopy compared to that obtained from XFM. Confocal microscopy revealed several small accumulations of the TAMRA-labeled DNA oligonucleotides within the cytoplasm and a stronger signal aligned with the nucleus. XFM analysis revealed a distribution of titanium that was very similar to that of TAMRA. The phosphorus map also revealed a strong co-localization with titanium and TAMRA. This is probably an artifact due to the fixing, staining, and mounting techniques involved in sample preparation. Titanium concentration, however, was determined only by the presence of nanoparticles. Figure 6B shows quantification of the number of nanoparticles located within the specified regions of interest (ROI). ROI 1 corresponds to a detectable XFM titanium signal (3.1×10^4 nanoparticles) although the TAMRA signal of this nanoparticle accumulation was only very weakly visible. Each nanoparticle was modified by approximately 2 TAMRA labeled oligonucleotides so that the optically fluorescent signal corresponds to 6.2×10^4 TAMRA molecules. The strongest titanium signal came from ROI 3 and showed the presence of approximately 1.3×10^6 nanoparticles. Confocal microscopy also showed a clearly detectable TAMRA signal within the same relative subcellular area. There are several titanium distributions obtained by XFM that were not imaged by confocal microscopy. This is likely due to the fact that the hard X-rays used in XFM are able to penetrate the entire cell, while confocal microscopy imaged optical cell slices of 0.13-μm thickness. To verify this, multiple planes of cells treated with ARS labeled TiO₂-DNA nanoconjugates were visualized by confocal microscopy and subsequently imaged by XFM. Results showed that accumulations of the ARS-labeled TiO₂-DNA nanoconjugates were not visible in one plane of

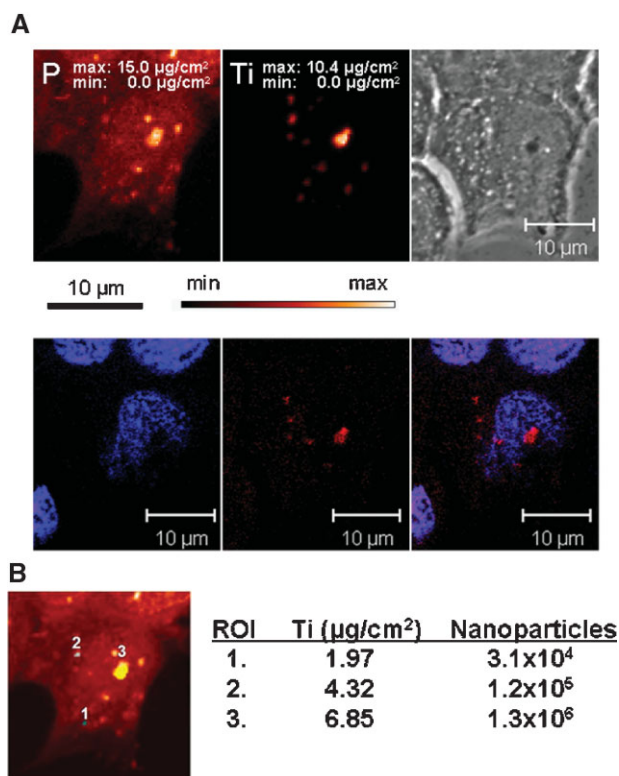


Figure 6. Combined use of XFM and confocal microscopy. A) Relative stability of TiO₂-DNA nanoconjugates. MCF-7 cells were transfected with TAMRA-labeled TiO₂-DNA nanoconjugates, sorted, and seeded on EM grids. Cells were then visualized by fluorescent confocal microscopy with a 0.13- μm optical slice (bottom row) and finally analyzed by XFM. Top left and center are the images of phosphorus (P) and titanium (Ti), respectively, obtained by XFM. Black bar is 10 μm (XFM), white bar is 10 μm (confocal images). B) Quantitative analysis of regions of interest (ROI). Several ROIs (defined by MAPS software) were analyzed to quantify levels of titanium. Concentration of titanium ($\mu\text{g cm}^{-2}$) is given as an average per ROI pixel. The number of nanoparticles per ROI was calculated by normalizing titanium concentrations by area, subtracting background ROI signals, and counting each 5-nm TiO₂ nanoparticle as 1400 titanium atoms.

microscopy but were visible in different planes. At the same time, however, both of the aggregates were shown to overlap with titanium (Figure 7). As few as 7.9×10^4 nanoparticles were detectable by fluorescence microscopy when 44% of the total surface of the TiO₂ nanoparticle was coated with ARS (Figure 7, ROI 1). The overall similarity in the distributions of both TAMRA labeled DNA oligonucleotide and titanium nanoparticle strongly suggest that the integrity of the TiO₂-DNA nanoconjugates remains intact at the time point examined (12 h).

3. Conclusions

These results demonstrate that it is possible to fluorescently label TiO₂ nanoparticles in a simple and specific manner using ARS. Most excitingly, this labeling can be used both prior to nanoparticle treatment of cells, and after nanoparticle internalization and fixation. To our knowledge, this is the first report of fluorescently labeled TiO₂ uptake quantification in a

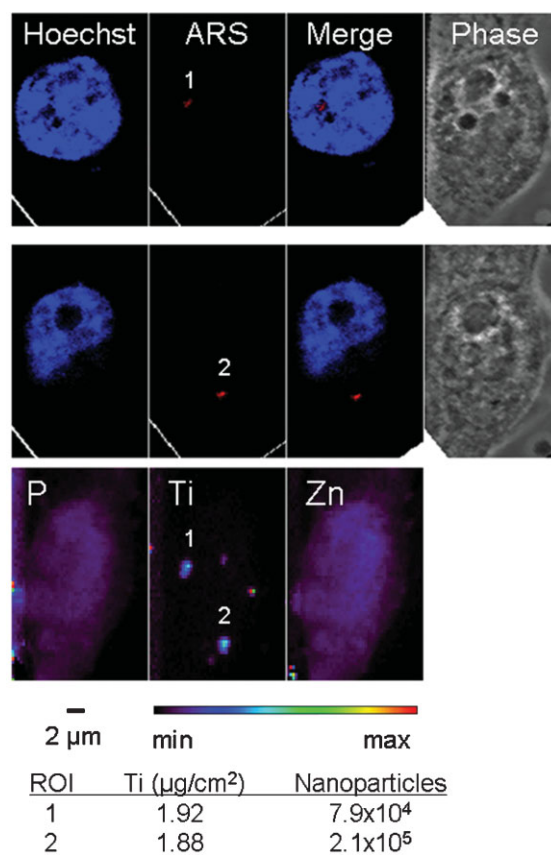


Figure 7. Multiplanar comparison of confocal microscopy and XFM. ARS-labeled TiO₂-DNA nanoconjugates were transfected in PC-3M cells. Confocal microscopy reveals in one plane the presence of ARS labeled nanoconjugates within the nucleus (ROI 1, top row) and another plane reveals localization in the cytoplasm (ROI 2, middle row). XFM (bottom row) reveals two strong intracellular titanium signals (ROIs 1 and 2), as well as several other smaller aggregates. Comparison suggests that the ARS signals overlap with the titanium distributions visualized by XFM.

large cell population (with assays using at least 10^4 cells per sample). This approach will allow for extensive study into the exact mechanisms by which these nanoparticles enter living cells, and the effects of potential future surface modifications. A similarly simple Alizarin Red S labeling should also be feasible for other semiconducting metal-oxide nanoparticles (e.g., Fe₂O₃, ZrO₂).^[18] Application of Alizarin Red S as a fluorescent label to other types of nanoparticles (e.g., carbon-based nanoparticles) would require more extensive conjugation chemistry. Localization of nanoparticles in tissues of treated animals should become optically visible using the ARS staining. In addition, we also showed that transfected TiO₂-DNA nanoconjugates remain stable in malignant cells for at least 12 h. The high sensitivity of XFM and the full sample penetration of the X-rays allowed detection of nanoparticles not visualized by microscopy. The combination of both techniques, however, did allow for validation of the ARS modification of the nanoparticles within cells, and it determined that as few as 7.9×10^4 ARS modified nanoparticles or as few as 3.1×10^4 nanoparticles modified by 6.2×10^4 TAMRA labeled oligonucleotides were detectable by fluorescent microscopy.

4. Experimental Section

Nanoconjugate preparation: All reagents were purchased from Sigma Aldrich unless otherwise specified. TiO₂ nanoparticles with mean diameters of around 5–6 nm were synthesized at Northwestern University's Nanofabrication Core of NU-Center for Cancer Nanotechnology Excellence, applying low-temperature alkaline hydrolysis route, dialyzed, and stored in Na₂HPO₄ buffer (10 mM) at 4 °C. Surface coating with glycidyl isopropyl ether was performed as described previously.^[9] Conjugation of single stranded 5' carboxyl deoxythymidine modified DNA oligonucleotides (ttcttgatgtggt) (The Midland Certified Reagent Co.) to dopamine, and subsequent conjugation to TiO₂ nanoparticles was performed as described previously.^[9,10,20] The oligonucleotides were also purchased with either tetramethylrhodamine (TAMRA) or Cy5 3' end modification.

Alizarin Red S surface coating and UV/vis absorbance spectrum analysis: For determination of covalent surface modification, TiO₂ nanoparticles (5 μm) were dialyzed and stored in Na₂HPO₄ buffer (10 mM) and mixed with Alizarin Red S (0.9 mM). The samples were then analyzed by the Nanodrop ND-1000 Spectrophotometer (NanoDrop Technologies Inc.) for absorbances ranging from 200–750 nm.

Cell culture and treatment with nanoparticles/nanoconjugates: All cell culture reagents were purchased from Mediatech Inc. unless otherwise specified. PC-3M metastatic prostate cancer cells were a gift from Dr. Raymond Bergan, Northwestern University. MCF-7/WS8 cells were obtained from American Type Culture Collection (ATCC). Both cell lines were maintained at 37 °C with 5% CO₂ in RPMI 1640 media supplemented with fetal bovine serum (10%), L-glutamine (2 mM), HEPES (10 mM), penicillin (100 I.U. mL⁻¹), streptomycin (100 μg mL⁻¹). MCF-7 cells were further supplemented with non-essential amino acids (1X), amphotericin B (0.25 μg mL⁻¹), and insulin (0.1 mg mL⁻¹) (Sigma-Aldrich). PC-3M cells were further supplemented with G418 sulfate (0.15 mg mL⁻¹). For treatment, cells were washed with phosphate buffered saline solution (PBS) and placed in serum free RPMI 1640 for 1–2 h. Then cells were treated with TiO₂ nanoparticles (333 nm) coated with or without ARS (60 μm), and/or oligonucleotides (160 μm) for 1 h. After treatment, cells were washed with PBS, and then in glycine (200 mM, pH 4) (Sigma Aldrich). After more washing in PBS, the cells were further prepared as described below, depending on the technique performed. Transfection of cells was carried out using Superfect (Qiagen) according to manufacturer's suggestions.

Flow cytometry and cell sorting: Cells to be analyzed by flow cytometry were grown until approximately 60% confluence. After treatment and washing, cells were trypsinized, collected in FBS supplemented medium, and brought to a single cell suspension. To determine cell viability, cell samples were treated with DAPI (5 μg mL⁻¹) (Molecular Probes, Invitrogen) prior to analysis. Samples were then taken to the Northwestern University Flow Cytometry Core Facility of the Robert H. Lurie Cancer Center to be analyzed or sorted on the DakoCytomation MoFlo Flow Cytometer (Dako). Excitation lasers of 350 nm and 543 nm were used to excite DAPI and TAMRA/ARS, respectively. Debris was excluded based on the forward and side scatter characteristics of the cell

populations. Analysis of flow cytometry data was performed using the FCS Express V3 program (De Novo Software).

Confocal microscopy: For visualization by confocal microscopy, cells were cultured on glass coverslips. Cells at approximately 60% confluence were treated and washed as described above. The cells were then fixed in paraformaldehyde (4%), and stained with Hoechst 33343 (Molecular Probes, Invitrogen). After washing the cells were placed in antifade mounting medium (Molecular Probes, Invitrogen) and visualized using the LSM 510 UV Meta Microscope (Carl Zeiss, Inc.) at the Northwestern University Cell Imaging Facilities using 405-nm, 488-nm, and 543-nm lasers with band-pass filters of 420–480 nm, 505–530 nm, and 560–615 nm, respectively.

XFM: Cells transfected with TiO₂-DNA (TAMRA) nanoconjugates were sorted for the presence of TAMRA, seeded on formvar coated gold EM grids (Electron Microscopy Sciences) and allowed to adhere. The samples were then fixed in cold methanol (–20 °C), and stained with Hoechst 33342 dye. The samples were placed in antifade mounting medium between a glass coverslip and slide, and imaged by confocal microscopy. Next, the cells were washed in glycine and PBS, dehydrated in ethanol (100%), and allowed to air dry. Before XFM analysis, the presence of the cells was verified, and coordinates for their locations were obtained by the Leica DMXRE light microscope and a motorized x/y stage (Ludl Electronic Products). XFM was performed at the 2-ID-D beamline at the Advanced Photon Source at Argonne National Laboratories where an undulator source was used to create hard X-rays with energies of 10 keV and focused using Fresnel zone plate optics. Emitted X-ray fluorescence was detected using an energy-dispersive germanium detector (LEGe Detector, Canberra). Elemental quantification and localizations were calculated using the MAPS program.^[50]

Acknowledgements

The authors would like to thank James Marvin, Jeffrey Nelson, and Paul Mehl of the Northwestern University Flow Cytometry Core Facility of the Robert H. Lurie Cancer Center. Northwestern University's Center for Cancer Nanotechnology Excellence (CCNE) Nanofabrication Core facility is thanked for preparation of nanoparticles. Use of the Advanced Photon Source was supported by the U.S. Department of Energy, Basic Energy Sciences, Office of Science, under Contract number DE-AC02-06CH11357. Work was supported by NIH Grants: CA107467, EB002100, P50 CA89018, U54CA119341.

- [1] D. M. Blake, P. C. Maness, Z. Huang, E. J. Wolfrum, J. Huang, W. A. Jacoby, *Separation and Purification Methods* **1999**, *28*, 1–50.
- [2] G. Gogniat, M. Thyssen, M. Denis, C. Pulgarin, S. Dukan, *FEMS Microbiol. Lett.* **2006**, *258*, 18–24.
- [3] Y. H. Tsuang, J. S. Sun, Y. C. Huang, C. H. Lu, W. H. Chang, C. C. Wang, *Artif. Organs* **2008**, *32*, 167–174.
- [4] H. P. Wu, T. L. Cheng, W. L. Tseng, *Langmuir* **2007**, *23*, 7880–7885.

- [5] J. M. Ashcroft, W. Gu, T. Zhang, S. M. Hughes, K. B. Hartman, C. Hofmann, A. G. Kanaras, D. A. Kilcoyne, M. Le Gros, Y. Yin, A. P. Alivisatos, C. A. Larabell, *Chem. Commun.* **2008**, 21, 2471–2473.
- [6] A. P. Zhang, Y. P. Sun, *World J. Gastroenterol.* **2004**, 10, 3191–3193.
- [7] R. Cai, Y. Kubota, T. Shuin, H. Sakai, K. Hashimoto, A. Fujishima, *Cancer Res.* **1992**, 52, 2346–2348.
- [8] J. W. Seo, H. Chung, M. Y. Kim, J. Lee, I. H. Choi, J. Cheon, *Small* **2007**, 3, 850–853.
- [9] T. Paunesku, T. Rajh, G. Wiederrecht, J. Maser, S. Vogt, N. Stojicevic, M. Protic, B. Lai, J. Oryhon, M. Thurnauer, G. Woloschak, *Nat. Mater.* **2003**, 2, 343–346.
- [10] T. Paunesku, S. Vogt, B. Lai, J. Maser, N. Stojicevic, K. T. Thurn, C. Osipo, H. Liu, D. Legnini, Z. Wang, C. Lee, G. E. Woloschak, *Nano Lett.* **2007**, 7, 596–601.
- [11] J. Liu, Z. Saponijc, N. M. Dimitrijevic, S. Luo, D. Preuss, T. Rajh, *Proc. SPIE* **2006**, 6096, 60960-F1-60960-F10.
- [12] N. P. Huang, M. H. Xu, C. W. Yuan, R. R. Yu, *J. Photochem. Photobiol. A: Chem.* **1997**, 108, 229–233.
- [13] T. C. Long, J. Tajuba, P. Sama, N. Saleh, C. Swartz, J. Parker, S. Hester, G. V. Lowry, B. Veronesi, *Environ. Health Perspect.* **2007**, 115, 1631–1637.
- [14] S. Singh, T. Shi, R. Duffin, C. Albrecht, D. van Berlo, D. Hohn, B. Fubini, G. Martra, I. Fenoglio, P. J. Borm, R. P. Schins, *Toxicol. Appl. Pharmacol.* **2007**, 222, 141–151.
- [15] H. A. Jeng, J. Swanson, *J. Environ. Sci. Health A Tox. Hazard Subst. Environ. Eng.* **2006**, 41, 2699–2711.
- [16] K. Peters, R. E. Unger, C. J. Kirkpatrick, A. M. Gatti, E. Monari, *J. Mater. Sci. Mater. Med.* **2004**, 15, 321–325.
- [17] E. Fabian, R. Landsiedel, L. Ma-Hock, K. Wiench, W. Wohlleben, B. van Ravenzwaay, *Arch. Toxicol.* **2008**, 82, 151–157.
- [18] T. Rajh, L. X. Chen, K. Lukas, T. Liu, M. C. Thurnauer, D. M. Tiede, *J. Phys. Chem. B* **2002**, 106, 10543–10552.
- [19] T. Rajh, J. M. Nedeljkovic, L. X. Chen, O. Poluektov, M. C. Thurnauer, *J. Phys. Chem. B* **1999**, 103, 3515–3519.
- [20] T. Rajh, Z. Saponijc, J. Liu, N. M. Dimitrijevic, N. F. Scherer, M. Vega-Arroyo, P. Zapol, L. A. Curtiss, M. C. Thurnauer, *Nano Lett.* **2004**, 4, 1017–1023.
- [21] J. Liu, L. de la Garza, L. Zhang, N. M. Dimitrijevic, X. Zuo, D. M. Tiede, T. Rajh, *Chem. Phys.* **2007**, 339, 154–163.
- [22] I. B. Weinstein, A. K. Joe, *Nat. Clin. Pract. Oncol.* **2006**, 3, 448–457.
- [23] Y. H. Wang, S. Liu, G. Zhang, C. Q. Zhou, H. X. Zhu, X. B. Zhou, L. P. Quan, J. F. Bai, N. Z. Xu, *Breast Cancer Res.* **2005**, 7, R220–R228.
- [24] D. W. Felsner, *Nat. Rev. Cancer* **2003**, 3, 375–380.
- [25] L. Chin, A. Tam, J. Pomerantz, M. Wong, J. Holash, N. Bardeesy, Q. Shen, R. O'Hagan, J. Pantginis, H. Zhou, J. W. Horner, 2nd, C. Cordon-Cardo, G. D. Yancopoulos, R. A. DePinho, *Nature* **1999**, 400, 468–472.
- [26] P. J. Endres, T. Paunesku, S. Vogt, T. J. Meade, G. E. Woloschak, *J. Am. Chem. Soc.* **2007**, 129, 15760–15761.
- [27] T. Paunesku, T. Ke, R. Dharmakumar, N. Mascheri, A. Wu, B. Lai, S. Vogt, J. Maser, K. Thurn, B. Szolc-Kowalska, A. Larson, R. C. Bergan, R. Omary, D. Li, Z.-R. Lu, G. E. Woloschak, *Nanomedicine* **2008**, 4, 201–207.
- [28] B. M. Rothen-Rutishauser, S. Schurch, B. Haenni, N. Kapp, P. Gehr, *Environ. Sci. Technol.* **2006**, 40, 4353–4359.
- [29] M. Geiser, M. Casaulta, B. Kupferschmid, H. Schulz, M. Semmler-Behnke, W. Kreyling, *Am. J. Respir. Cell Mol. Biol.* **2008**, 38, 371–376.
- [30] H. Suzuki, T. Toyooka, Y. Ibuki, *Environ. Sci. Technol.* **2007**, 41, 3018–3024.
- [31] J. L. Haynes, *Cytometry. Suppl.* **1988**, 3, 7–17.
- [32] C. J. Fahrni, *Curr. Opin. Chem. Biol.* **2007**, 11, 121–127.
- [33] T. Paunesku, S. Vogt, J. Maser, B. Lai, G. Woloschak, *J. Cell. Biochem.* **2006**, 99, 1489–1502.
- [34] R. McRae, B. Lai, S. Vogt, C. J. Fahrni, *J. Struct. Biol.* **2006**, 155, 22–29.
- [35] L. Yang, R. McRae, M. M. Henary, R. Patel, B. Lai, S. Vogt, C. J. Fahrni, *Proc. Natl. Acad. Sci. U. S. A.* **2005**, 102, 11179–11184.
- [36] T. Rajh, O. Poluektov, A. A. Dubinski, G. Wiederrecht, M. C. Thurnauer, A. D. Trifunac, *Chem. Phys. Lett.* **2001**, 344, 31.
- [37] V. Papalexiou, A. B. Novaes, Jr., M. F. Grisi, S. S. Souza, M. Taba, Jr., J. K. Kajiwara, *Clin. Oral Implants Res.* **2004**, 15, 44–53.
- [38] H. Puchtler, S. N. Meloan, M. S. Terry, *J. Histochem. Cytochem.* **1969**, 17, 110–124.
- [39] H. Zhong, N. Li, F. Zhao, K. A. Li, *Talanta* **2004**, 62, 37.
- [40] R. Huber, S. Sporlein, J. E. Moser, M. Gratzel, J. Wachtveitl, *J. Phys. Chem. B* **2000**, 104, 8995–9003.
- [41] C. Morassutti, B. Scaggiante, B. Dapas, L. Xodo, G. Tell, F. Quadrioglio, *Biochimie* **1999**, 81, 1115.
- [42] E. R. Whittmore, D. T. Loo, J. A. Watt, C. W. Cotmans, *Neuroscience* **1995**, 67, 921–932.
- [43] P. P. Laktionov, J. E. Dazard, E. Vives, E. Y. Rykova, J. Piette, V. V. Vlassov, B. Lebleu, *Nucleic Acids Res.* **1999**, 27, 2315–2324.
- [44] F. O. Nestle, R. S. Mitra, C. F. Bennett, H. Chan, B. J. Nickoloff, *J. Invest. Dermatol.* **1994**, 103, 569–575.
- [45] S. B. Noonberg, M. R. Garovoy, C. A. Hunt, *J. Invest. Dermatol.* **1993**, 101, 727–731.
- [46] P. de Diesbach, F. N'Kuli, C. Berens, E. Sonveaux, M. Monsigny, A. C. Roche, P. J. Courtoy, *Nucleic Acids Res.* **2002**, 30, 1512–1521.
- [47] C. Garcia-Chaumont, O. Seksek, J. Grzybowska, E. Borowski, J. Bolard, *Pharmacol. Ther.* **2000**, 87, 255–277.
- [48] M. A. Lysik, S. Wu-Pong, *J. Pharm. Sci.* **2003**, 92, 1559–1573.
- [49] I. A. Khalil, K. Kogure, H. Akita, H. Harashima, *Pharmacol. Rev.* **2006**, 58, 32–45.
- [50] S. Vogt, *J. Phys. IV* **2003**, 104, 635–638.

Received: October 4, 2008
Published online: February 25, 2009